WILEY-VCH

Article type: Communication

Percolation Threshold Enables Optical Resistive-Memory Switching and Light-Tuneable Synaptic Learning in Segregated Nanocomposites

Ayoub H. Jaafar,[a,b] Mary O'Neill,[a,c] Stephen M. Kelly,[d] Emanuele Verrelli[a],* and Neil T. Kemp[a],*

[a] Department of Physics and Mathematics, University of Hull, Cottingham Rd, HU6 7RX,

Hull, United Kingdom

[b] Physics Department, College of Science, University of Baghdad, Baghdad, Iraq

[c] School of Science and Technology, Nottingham Trent University, Clifton Lane, NG11 8NS,

Nottingham, United Kingdom

[d] Department of Chemistry and Biochemistry, University of Hull, Cottingham Rd, HU6 7RX,

Hull, United Kingdom

* Authors to whom correspondence should be addressed. Electronic mail:

N.Kemp@hull.ac.uk, E.Verrelli@hull.ac.uk

An optical memristor is demonstrated where, the electrical resistance memory depends on the

history of both the current flowing through the device and the irradiance of incident light onto

it. It is based on a nanocomposite consisting of functionalized gold nanoparticles in an optically

active azobenzene polymer matrix. The composite has an extremely low percolation threshold

of 0.04% by volume for conductivity, because of the aggregation of the conducting nanoparticles into filamentary nano-channels. Optical irradiation results in photomechanical switching by expansion of the thin film from above to below the percolation threshold giving a large LOW/HIGH resistance ratio of 10^3. The device acts as an artificial synapse, whose conductivity or plasticity can be independently modulated, either electrically or optically, to enable tuneable and reconfigurable synaptic circuits for brain-inspired artificial intelligent or visual memory arrays. The lifetime of the resistive memory states is also optically controllable, which would enable spatial modulation of long- and short-term memory.

Leon Chua's pioneering work on the theoretical description of memristors,[1] combined with their potential applications in next generation logic circuits and memory devices, has sparked enormous interest in low-power, non-volatile, two-terminal resistive memory devices.[2],[3],[4],[5],[6],[7] The ability of memristors to emulate the analogue switching and learning properties of biological synapses[8],[9],[10],[11] is also emerging as a significant area of importance that has the potential to usher in a new generation of large scale bio-inspired neural networks. In recent years memristor performance has advanced considerably. Very high levels of endurance (120 billion cycles) and retention have been achieved, and ultra-high density cross bar arrays have been realized with scalability down to ~2 nm.[12] Key challenges however remain, such as variability between devices when programming to the same desired state and long device access times (latency), which is currently preventing memristive based neuromorphic hardware from going mainstream.[13]

The optical control of memristors is gaining interest as a means to spatially and temporally switch or fine-tune the electronic properties of devices to the desired specifications. Numerous potential applications are anticipated, including optical signaling and switchable memory elements in optical communications and photonic integrated circuits, light sensors, fast parallel

reset of memory banks, etc. To date, relatively few optical memristors have been reported, with most applying photoconductive effects, inherent to many semiconductors, to induce resistive memory switching.[14],[15] For example, a photocurrent has been used to shift the resistance of the high- and low-resistive switching states, as well as the threshold voltage for switching.[16],[17],[18] In these devices the optical and electrical switching have similar origins and result from the charging and discharging of the same long-lived trapped states, which raise and lower the barrier for charge transport across an interface. Memory logic operations have been obtained by combining electrical and optical pulses.[19],[20],[21] The transmission of plasmonically coupled light through a waveguide was modulated by resistive switching in a plasmonic memristor.[22],[23]

In a recent publication we demonstrated reversible and latched optical switching of a resistive memory device.[24] Intriguingly, the optical effect, as well as the electronic effect, is integrative: the resistance depends on the cumulative optical energy onto the device as well as the cumulative current. The optical effect enables dynamic control of the memristor's learning properties, including optical switching between short-term and long-term memory and optical control of the synaptic efficacy, opening the way to new, optically reconfigurable neural network circuits.[24] The device was enabled by depositing an optically active azobenzene polymer material onto a vertical array of resistive-switching ZnO nanorods. Illumination induces *trans-/ cis* isomerization of the azobenzene groups, which expands or contracts the polymer layer and alters the resistance of the low/high states and retention time. However the LOW/HIGH ratio, i.e. the ratio between the resistivity values of the two resistive memory states, is low, ≈10, and optical irradiation shifts the resistance of both states, rather than significantly changing the LOW/HIGH ratio. A more promising approach is the optical modulation of the plasticity of only one of the memory states. This requires the two memory states to respond differently, so the standard approach of defects charging/discharging is not viable. We adopt a

completely different approach exploiting percolation thresholds in nanocomposites to maximize the LOW/HIGH ratio. This is achieved by a new, segregated nanocomposite material, which displays resistive memory switching behavior. The nanocomposite consists of spherical gold nanoparticles (NPs) distributed in a photoactive polymer, which aggregate into conducting nano-channels forming percolation pathways across the layer. The unique properties of this nanocomposite are optimal at a filler volume fraction just above the percolation threshold, which is extremely low because of segregation. Expansion of the host, on irradiation with light, reduces the effective filler volume fraction below the percolation threshold, causing a large drop in conductivity of the HRS. The conductivity of the LRS state is hardly changed by the photomechanical expansion. Hence, a tri-stable memristor is obtained with a common low resistance state and an optically switchable HRS, giving an LOW/HIGH ratio of up to 10^3 under illumination. This is the first time that percolation has been applied to an optical memristor, although a photomechanical switching of conductivity across a percolation threshold has previously been reported.[25],[26]

Figure 1a) shows a schematic of the device, consisting of a single layer of a photoactive azobenzene polymer, *poly*(disperse red 1 acrylate) (PDR1A), containing functionalized gold NPs of diameter 6-7 nm sandwiched between electrodes of ITO and aluminium. PDR1A undergoes a reversible *trans-cis-trans* photochemical isomerization upon optical excitation,[27],[28],[29] as shown in Figure 1b. This isomerization results in the photoinduced expansion and contraction of the thin film, as illustrated in Figure 1c for the undoped PDR1A sample. The absorption probability of the azobenzene chromophore is greatest when its transition moment is parallel to the electric field of the incident wave. The excited molecules reorient to a position that is independent of their original orientation.[30] This reorientation is enhanced by configurational changes, since isomerization from the *trans-* to the *cis* isomer reduces the molecular volume.[31] When circularly polarized light is incident, only

4

chromophores aligned in the plane of the layer are re-oriented, so that the out-of-plane chromophore distribution increases with time, leading to an expansion of the thin film. The observed increase in the thickness is ~20%, which is consistent with previous reports.[32] On removal of the light, *cis-trans* isomerisation occurs spontaneously, so the film thermally relaxes to its original thickness within 150 minutes, as the equilibrium chromophore distribution is restored. Similarly excitation with linearly polarized light restores some in-plane alignment, as the in-plane chromophores, which have a transition moment perpendicular to the electric field of the beam, cannot be reoriented by the polarized light. This forced relaxation restores the film to its original thickness in 15 minutes.

Figure 2a shows the conductivity of the gold NP doped samples, 1 to 6 (see table S1), as a function of the gold NP volume fraction. There is a sharp increase of conductivity, over three orders of magnitude, when the volume fraction increases from 0.033% (sample 2) to 0.065% (sample 3). Such behaviour is expected from the physical phenomenon of percolation, where above a certain critical threshold, the conducting filler forms conductive paths in an inert host. These connect the two electrodes of the device, effectively short-circuiting the device itself. The critical filler fraction is also often referred to as the percolation threshold. The super-critical (sub-critical) regime notation refers to filler fraction values above (below) the percolation threshold, respectively. The DC conductivity of the system can be approximated by a power law given by the following equation.[33]

$$\sigma_{DC}(f) = \begin{cases} \sigma_{DC}^{filler}(f - f_c)^t, f > f_c \\ \sigma_{DC}^{host}(f_c - f)^{-s}, f < f_c \end{cases} \tag{1}$$

where σ_{DC}^{filler} and σ_{DC}^{host} are constants related to the conductivities of the filler and host respectively, f_c is the percolation threshold and t and s are the super- and sub-critical percolation exponents, respectively. Equation 1 can be regarded as a simplified phenomenological

approximation to a more complex law.[34] The pink curve in Figure 2a represents a plot of the supercritical function of equation 1 and shows a good match to the experimental percolation regime, with a percolation threshold of 0.04% and a super-critical exponent $t = 1$. A striking feature of these data is that the percolation threshold is extremely low for a spherical filler. Indeed, the percolation threshold for 3D films of homogeneous nanocomposites with spherical fillers is estimated[35] experimentally and theoretically to be ~20%. The low threshold found here compares well with those obtained for nanocomposite materials doped with conducting fibers, such as metal nanowires[36],[37] or carbon fibers,[38] where both anisotropy and alignment enables electrical connectivity at much lower filler concentrations. In these materials the critical percolation threshold can decrease by 2-3 orders of magnitude, to a value as low as 0.032%,[39] by changing the aspect ratio.[39],[40],[41] A very low percolation threshold of 0.025% was achieved for spherical organic conducting nanoparticles, doped in an inert polymer matrix by segregation due to self-assembly.[42] We suggest that the percolation behaviour shown in Figure 2a with a very low percolation threshold provides indirect experimental evidence for an inhomogeneous nanocomposite, where the NPs segregate into conducting ribbon-like pathways. The images in Figure 2a illustrate the concept. Below threshold, the concentration of NPs is too low to bridge the thin film. At percolation threshold, one or more bridging pathways are formed and these are extended as the concentration of NPs is increased above threshold. TEM images of the thin film of sample 3 support the hypothesis. Figure 2b shows the image of the NP-doped PDR1A film, capped with a metal layer (lower left) that was deposited following thermal annealing of the film at 95°C for 8 hours. The NPs are not homogeneously distributed, but are mostly located at what was the polymer/air interface. Similar segregation has been reported in a number of systems and has been attributed to competing enthalpic and entropic processes during thermal annealing.[43],[44],[45] The film also shows discrete regions, where filamentary pathways or extended clusters of NPs traverse across the polymer layer between the two electrodes. We suggest that these are the origin of the percolation nano-channels across which

electrons can tunnel. It is beyond the scope of this paper to explain how and why ribbon-like filaments are formed. One possibility might be incomplete migration to the surface of a randomly formed NP aggregate pinned to a void or defect in the bulk of the film.[46] However, these regions are not extensive and most of the bulk contains very few NPs, as shown in **Figure S1** in the supporting information.

The Au NP:PDR1A nanocomposite material exhibits bipolar resistive memory switching using electronic stimuli. **Figure 3a** shows current-voltage (I-V) curves obtained by performing symmetric bias sweeps on an initially fresh device on sample 3. The device is initially found in its HRS state and a (SET) transition to the low resistance state (LRS) is observed at ~+0.4 V, while the opposite (RESET) transition has an onset bias of ~-0.4V and is much smoother than the SET one. The SET transition always takes place at positive biases, while the RESET one always occurs at negative biases. The phenomenon is highly reproducible, as demonstrated by the overlapping I-V cycles shown in Figure 3a. **Figure 3b** shows that the ON/OFF ratio, i.e. the ratio between the LRS and HRS conductivity values is maximum, equal to about 300, for sample 3, i.e. just above the percolation threshold. When the gold NP volume fraction is higher, the HRS has a large current due to multiple percolating pathways, see **Figure S2** of the supporting information, which shows the I-V characteristics of samples with different gold nanoparticle concentrations. Both the LRS and HRS state of sample 2, whose gold NP concentration is below the percolation threshold, are of low conductivity whilst sample 1 and the PDR1A host do not show any resistive switching. It is beyond the scope of this work to precisely understand the physical mechanism behind the resistive switching observed in Figure 3a. However, **Figure S2** shows that both the HRS and LRS states of all samples seem to be 1) ohmic (see Figure S2b) and 2) with a zero bias at zero current crossing for both forward and backward bias sweeps (see Figure S2a). These two features show the absence of any measurable dynamic charge trapping, since the presence of any trapped charges that are dynamically

injected and extracted from the film would result in a more complex I-V behaviour[47] and the I-V sweeps would show hysteresis with subsequent mismatch in the zero current crossing between forward and backward sweeps.[48],[49] It is worth noting though that charge trapping has been suggested as a switching mechanism for polymer-metallic NP resistive switching memories elsewhere.[50] We have suggested above that the conductivity in the HRS originates from segregated gold nano-filaments. Perhaps the electrically induced LRS, which has a significantly higher conductivity than the fresh devices is related to some sort of structural and morphological change of the percolation path, e.g. migration of gold nanoparticles from the interface to the bulk so creating extra conducting nano-filaments, that could be responsible for an increased conductivity by 2-3 orders of magnitude as compared to that of the HRS (or fresh percolating devices). *Cis-trans* isomerisation of the PDR1A host creates free volume, which may enable such reconfiguration. At this stage more investigations are required in order to elucidate this point.

Figure 3c demonstrates the optoelectronic response of a gold NP-doped PDR1A device with the NP concentration tuned to just above the percolation threshold. As shown in Figure 1c above, for the undoped PDR1A, irradiation of the sample using circularly polarized light for 30 minutes induces a photomechanical response leading to an expansion of the sample by about 20%. This breaks the filamentary conducting pathways, causing a large decrease (almost 3 orders of magnitude) in the device's conductivity (red arrow represents the change in conductivity) from a high resistance state (HRS) to an optically enhanced high resistance state, denoted HRS$_{opt}$. The extremely large optical modulation happens because the operating conditions of the device are effectively migrating across the percolation threshold, from a supercritical condition to a subcritical one. This is illustrated in the schematic diagram of Figure 3c, which shows that the average inter-particle distance increases as the PDR1A is stretched on irradiation. It is beyond the scope of this paper to elucidate how the NPs themselves move under irradiation. The expansion of the thin film is reversible on irradiation with linearly polarized

light, shifting the device conductivity back to its original value (green arrow). A typical conductivity transient during the transition is shown in Figure 3d. For irradiation with circularly polarized (linearly polarized) light of constant intensity, the conductivity drops (increases) as a function of time to a minimum (maximum) saturated level, reflecting the changes in film thickness. The presence of plateaus and sharp transitions in conductivity during irradiation may indicate that the expansion and contraction causes the breaking and connection of individual percolation pathways.

The photomechanical and electronic responses are combined in the optical memristor, whose current-voltage characteristics are illustrated in **Figure 4a**. Interestingly the LRS is hardly affected by optical modulation of the resistive switching device. Here the I-V sweeps, shown in red, are recorded at the end of a film expansion, resulting from 15 minutes irradiation with circularly polarized light, whilst the green sweeps are made after the film is fully relaxed. It should be noted that the SET transition in an expanded film takes place at a bias that is slightly, but reproducibly and consistently higher than that in a fully relaxed condition, +0.6V and +0.4V respectively. The switching is highly reproducible as shown in **Figure S3**. Figure 4b gives a more detailed view of the temporal evolution of the conductivities of the HRS and LRS during photoinduced expansion and relaxation cycles. The integrating effect is observed: the conductivity increases (decreases) as a function of time although the irradiance of the incident circularly polarized (linearly polarized) beam remains constant. The maximum reduction of over two orders of magnitude occurs after 30 minutes irradiation, see red dashed line in Figure 4b. The conductivity of the HRS is linked to the breaking/reforming of percolation paths in the nanocomposite, i.e. compare with results in Figure 3d. The fact that the electronic LRS does not undergo any remarkable drop in conductivity as a result of film expansion clearly differentiates the LRS from the HRS. Noting from Figure 2b that many nanoparticles are located at the surface of the composite film, a tentative explanation can be given: NPs may be

electrically induced to migrate from the surface to the bulk to extend the percolating pathways in the LRS. This effectively creates a film with a higher bulk filler volume fraction. On expansion of the film, the conductivity of the HRS shifts from above to below percolation threshold, whilst it remains above threshold for the LRS. A tri-stable device has been created with a more-or-less optically independent LRS and an HRS, whose plasticity (conductivity) can be significantly altered, depending on the intensity and the illumination period of the incident optical beam. The lifetime of the HRS_{opt} depends on the time taken for the expanded film to return to its relaxed state. Figure 4c compares the relaxation of HRS_{opt} to HRS achieved using linearly polarized irradiation (forced) and in the dark (thermal relaxation). The timescales for the relaxation of conductivity match those obtained for film contraction, see Figure 1c. Forced relaxation switches the device from the HRS_{opt} to the HRS in 900 s (15 min) while thermal relaxation is clearly much slower than that. Finally, it is shown that the memristor acts as a synapse, which "learns" by adapting to repeated signalling events. Spike-timing-dependent plasticity is used to quantify the learning, with plasticity monitored by changes in the electrical resistance, $\Delta G/G$, as a function of the time difference, Δt, between two electrical pulses of opposite polarity applied to the memristor,[51] see Figure 4d. ΔG is the difference in the conductance of the memristor before and after the double pulse. The figure shows that the plasticity varies as expected[52–54] with Δt, showing the learning potential of such a memristor neural network. The plasticity also increases significantly under irradiation with UV light, demonstrating the optical control of learning. The photomechanical polymer, PDR1A, was chosen just as a model system to demonstrate this unique optical memristor configuration, but it has the dual disadvantage of low optical sensitivity and a long response time. The sensitivity can be increased enormously, for example, by the replacement of PDR1A by a liquid crystalline azo–polymer to amplify the optical effect.[55] Similarly the optical response times can be significantly varied by molecular design.

In conclusion we have developed a tri-stable optical memristor with an extremely high LOW/HIGH resistance ratio by exploiting photoexpansion of a nanocomposite, containing conducting gold nanoparticle channels, to optically switch the HRS from above to below the percolation threshold. The nanocomposite morphology is assumed to change when the device is electrically set, so the LRS does not switch across the percolation threshold. We show that the device acts as an artificial synapse, where the plasticity and the lifetime of the HRS state can be optically controlled. The spatial and temporal patterning of such memristor arrays by light can be used to dynamically reconfigure neural circuits or modulate the learning properties of specific regions of artificial brain-like systems. The devices have the potential to mimic human visual memory, as they solve the key challenge of how to detect and store the image information.[56] Uniquely, the ability to optically control the lifetime by subsequent irradiation with a different pattern of linearly polarized light adds intriguing possibilities to temporally and spatially switch between long- and short-term memory.

Experimental Section

The schematic of the device, Figure 1a), consists of a single thin-film (200 nm thick) of the optically active and electronically conducting hybrid polymer/nanoparticle material sandwiched between conducting ITO and aluminium electrodes. The thin-film is made by mixing an optically active polymer, poly(disperse red 1 acrylate) (PDR1A) with gold nanoparticles (NPs) and depositing via a spin-coating procedure (1000 rpm for 30 s). The solution was made by mixing together two solutions, 5 % PDR1A (Sigma Aldrich) in tetrahydrofuran (weight/weight) and 1 % functionalized gold nanoparticles (NPs), diameter 6-7 nm (PlasmaChem) in toluene (weight/weight), with a blending ratio designed to a give predefined volume fraction of the gold nanoparticles in the PDR1A as discussed in the

11

supporting information. The thin-film was annealed at ~95°C for 8 hours. This migrates the gold nanoparticles to the polymer/air interface[43] and forms, in some places, conducting pathways that bridge (*via* inter nanoparticle electron tunnelling) between the top and bottom electrodes. The top metal contacts consist of 400 µm diameter circles of aluminium (200 nm thick), deposited by thermal evaporation. I-V sweeps (2 terminal) were carried out using a probe station equipped with an HP4140B source-meter unit. Photomechanical expansion/contraction was induced by irradiation with circular/linear polarized light from an Argon ion laser (514 nm) having a spot size of 3 mm and an average power per unit area across a single device of 180 mW/cm^2. A quarter wave plate was used to generate circularly polarized light form the linearly polarized laser output. TEM cross-section studies were carried out by fabricating the thin-film layered structured on top a of polished resin block, which was then covered in more resin and sectioned by microtome.

Supporting Information

Supporting Information is available from the Wiley Online Library or from the author.

Acknowledgements

References

[1]   L. O. Chua, *IEEE Trans. Circuit Theory* **1971**, *CT-18*, 507.

[2]   M.-J. Lee, C. B. Lee, D. Lee, S. R. Lee, M. Chang, J. H. Hur, Y.-B. Kim, C.-J. Kim, D. H. Seo, S. Seo, U.-I. Chung, I.-K. Yoo, K. Kim, *Nat. Mater.* **2011**, *10*, 625.

[3]   K.-H. K.-H. Kim, S. Gaba, D. Wheeler, J. M. Cruz-albrecht, T. Hussain, N. Srinivasa, W. Lu, *Nano Lett.* **2012**, *12*, 389.

[4]   A. Khiat, P. Ayliff, T. Prodromakis, *Sci. Rep.* **2016**, 1.

[5]   S. Pi, P. Lin, Q. Xia, *J. Vac. Sci. Technol. B Microelectron. Nanom. Struct.* **2013**, *31*, 06FA02.

[6]   E. Verrelli, R. J. Gray, M. O. Neill, S. M. Kelly, N. T. Kemp, *Mater. Res. Express* **2014**, *1*, 046305.

[7]   R. J. Gray, A. H. Jaafar, E. Verrelli, N. T. Kemp, *Thin Solid Films* **2018**, *662*, 116.

[8]   S. H. Jo, T. Chang, I. Ebong, B. B. Bhadviya, P. Mazumder, W. Lu, *Nano Lett.* **2010**, *10*, 1297.

[9]   L. O. Chua, *Nanotechnology* **2013**, *24*, 383001.

[10]   E. R. Kandel, *In Search of Memory*, W. Norton And Company, New York, **2006**.

[11]   I. Antonov, I. Antonova, E. R. Kandel, R. D. Hawkins, *Neuron* **2003**, *37*, 135.

[12]   S. Pi, C. Li, H. Jiang, W. Xia, H. Xin, J. J. Yang, Q. Xia, *Nat. Nanotechnol.* **2019**, *14*, 35.

[13]   G. C. Adam, A. Khiat, T. Prodromakis, *Nat. Commun.* **2018**, *9*, 2.

[14]   J. Park, S. Lee, J. Lee, K. Yong, K. Y. J. Park, S. Lee, J. Lee, *Adv. Mater.* **2013**, *25*,

6423.

[15]   A. Kathalingam, H.-S. Kim, S.-D. Kim, H.-C. Park, *Opt. Mater. (Amst).* **2015**, *48*, 190.

[16]   M. Ungureanu, R. Zazpe, F. Golmar, P. Stoliar, R. Llopis, F. Casanova, L. E. Hueso, *Adv. Mater.* **2012**, *24*, 2496.

[17]   A. Mehonic, T. Gerard, A. J. Kenyon, A. Mehonic, T. Gerard, A. J. Kenyon, *Appl. Phys. Lett.* **2017**, *233502*, DOI 10.1063/1.5009069.

[18]   A. Bera, H. Peng, J. Lourembam, Y. Shen, X. W. Sun, T. Wu, *Adv. Funct. Mater.* **2013**, *23*, 4977.

[19]   F. Zhou, Y. Liu, X. Shen, M. Wang, F. Yuan, Y. Chai, *Adv. Funct. Mater.* **2018**, *1800080*, 1.

[20]   H. Tan, G. Liu, H. Yang, X. Yi, L. Pan, J. Shang, S. Long, M. Liu, Y. Wu, R. Li, *ACS Nano* **2017**, *11*, 11298.

[21]   H. Tan, G. Liu, X. Zhu, H. Yang, B. Chen, X. Chen, J. Shang, W. D. Lu, Y. Wu, R. W. Li, *Adv. Mater.* **2015**, *27*, 2797.

[22]   A. Emboras, I. Goykhman, B. Desiatov, N. Mazurski, L. Stern, J. Shappir, U. Levy, *Nano Lett.* **2013**, *13*, 6151.

[23]   C. Hoessbacher, Y. Fedoryshyn, A. Emboras, A. Melikyan, M. Kohl, D. Hillerkuss, C. Hafner, J. Leuthold, *Optica* **2014**, *1*, 198.

[24]   A. H. Jaafar, R. J. Gray, E. Verrelli, M. O'Neill, S. M. Kelly, N. T. Kemp, *Nanoscale* **2017**, *9*, 17091.

[25]   V. Schneider, O. Polonskyi, T. Strunskus, M. Elbahri, F. Faupel, *Sci. Rep.* **2017**, *7*, 9648.

[26]   V. Schneider, T. Strunskus, M. Elbahri, F. Faupel, *Carbon N. Y.* **2015**, *90*, 94.

[27]   H. Rau, *In Photochemistry and Photophysics*, CRC Press, Boca Raton, FL, **1990**.

[28]   A. Natansohn, P. Rochon, *Chem. Rev.* **2002**, *102*, 4139.

[29]   O. M. Tanchak, C. J. Barrett, *Macromolecules* **2005**, *38*, 10566.

[30] M. O'Neill, S. M. Kelly, *J. Phys. D. Appl. Phys.* **2000**, *33*, R67.

[31] T. Kosa, P. Palffy-Muhoray, *Pure Appl. Opt. J. Eur. Opt. Soc. Part A* **1996**, *5*, 595.

[32] K. G. Yager, O. M. Tanchak, C. Godbout, H. Fritzsche, C. J. Barrett, *Macromolecules* **2006**, *39*, 9311.

[33] K. L. Chan, M. Mariatti, Z. Lockman, L. C. Sim, *J. Appl. Polym. Sci.* **2011**, *121*, 3145.

[34] J. Li, M. Ostling, *Nanoscale* **2015**, *7*, 3424.

[35] M. J. Powell, *Phys. Rev. B* **1979**, *20*, 4194.

[36] J. S. Park, T. Kim, W. S. Kim, *Sci. Rep.* **2017**, *7*.

[37] A. Lonjon, P. Demont, E. Dantras, C. Lacabanne, *J. Non. Cryst. Solids* **2012**, *358*, 3074.

[38] F. Sharif, M. Arjmand, A. A. Moud, U. Sundararaj, E. P. L. Roberts, *ACS Appl. Mater. Interfaces* **2017**, *9*, 14171.

[39] P. Wang, H. Chong, J. Zhang, H. Lu, *ACS Appl. Mater. Interfaces* **2017**, *9*, 22006.

[40] S. H. Munson-mcgee, *Phys. Rev. B* **1991**, *43*, 3331.

[41] S. S. Rahatekar, M. Hamm, M. S. P. Shaffer, J. A. Elliott, *J. Chem. Phys.* **2013**, *134702*, 18.

[42] P. Banerjee, B. M. Mandal, *Macromolecules* **1995**, *28*, 3940.

[43] S. Gupta, Q. Zhang, T. Emrick, A. C. Balazs, T. P. Russell, *Nat. Mater.* **2006**, *5*, 229.

[44] A. C. Balazs, T. Emrick, T. P. Russell, *Science (80-.).* **2006**, *314*, 1107.

[45] E. S. Mcgarrity, A. L. Frischknecht, M. E. Mackay, *J. Chem. Phys.* **2008**, *128*, 154904.

[46] J. Y. Lee, Q. Zhang, T. Emrick, A. J. Crosby, *Macromolecules* **2006**, *39*, 7392.

[47] E. Verrelli, D. Tsoukalas, *J. Appl. Phys.* **2013**, *114103*, DOI 10.1063/1.4795278.

[48] I. Thurzo, G. Pham, D. R. T. Zahn, *Chem. Phys.* **2003**, *287*, 43.

[49] P. H. Nguyen, S. Scheinert, S. Berleb, W. Brüiting, G. Paasch, *Org. Electron. physics, Mater. Appl.* **2001**, *2*, 105.

[50] J. Ouyang, *Org. Electron.* **2013**, *14*, 1458.

[51]   T. Serrano-Gotarredona, T. Masquelier, T. Prodromakis, G. Indiveri, B. Linares-Barranco, *Front. Neurosci.* **2013**, *7*, 1.

[52]   G. Q. Bi, M. M. Poo, *J. Neurosci.* **1998**, *18*, 10464.

[53]   W. Gerstner, R. Ritz, J. L. van Hemmen, *Biol. Cybern.* **1993**, *69*, 503.

[54]   L. I. Zhang, H. W. Tao, C. E. Holt, W. a Harris, M. Poo, *Nature* **1998**, *395*, 37.

[55]   H. K. Bisoyi, Q. Li, *Chem. Rev.* **2016**, *116*, 15089.

[56]   S. Chen, Z. Lou, D. Chen, G. Shen, *Adv. Mater.* **2018**, *1705400*, 1.
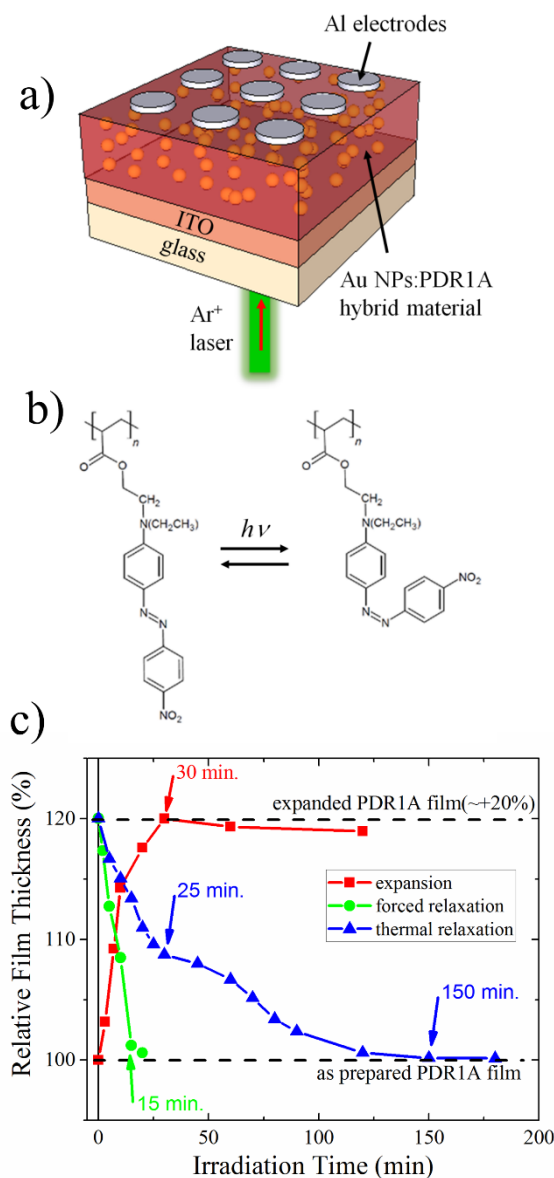
Figure 1. (a) Schematic of the optical memristor device consisting of Au nanoparticles (NPs) embedded within a thin film of azobenzene polymer poly(disperse red 1 acrylate (PDR1A) and deposited between ITO and Al electrodes. (b) The trans-cis photochemical isomerization of PDR1A. (c) Thickness changes of a PDR1A film with time on irradiation with (red line) circularly polarised light of intensity 180 mWcm^{-2}. The green and blue lines show film contraction of the expanded film with time, with (forced relaxation) and without (thermal relaxation) irradiation using linearly polarised light respectively.

17
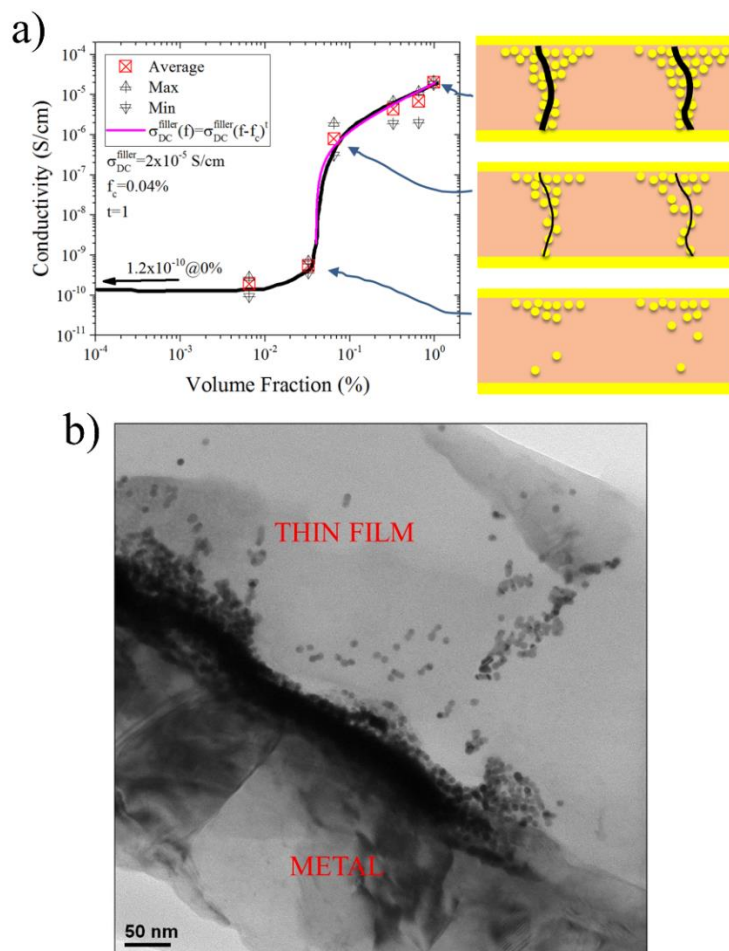
Figure 2. a) Conductivity of two terminal devices as a function of Au NP volume fraction in PDR1A. At each volume fraction, the data points shown in the graph represent the average, maximum and minimum conductivity of the nanocomposite film. The black curve represents a guide to the eye of the observed data trend. The pink curve represents a plot of the supercritical function given in Equation (1) showing a good match to the experimental percolation regime, assuming a percolation threshold of 0.04% and a super-critical exponent $t = 1$. The images illustrate the segregation of NPs below, at and above percolation threshold. b) TEM image of an annealed thin film of Au doped PDR1A of volume fraction 0.065%, showing the inhomogeneous distribution of NPs and the development of a filamentary pathway extending across most of the bulk film. The metal layer present in the lower left of the TEM image at this interface is added after thermal annealing to protect the device structure during cross-sectioning by microtome).
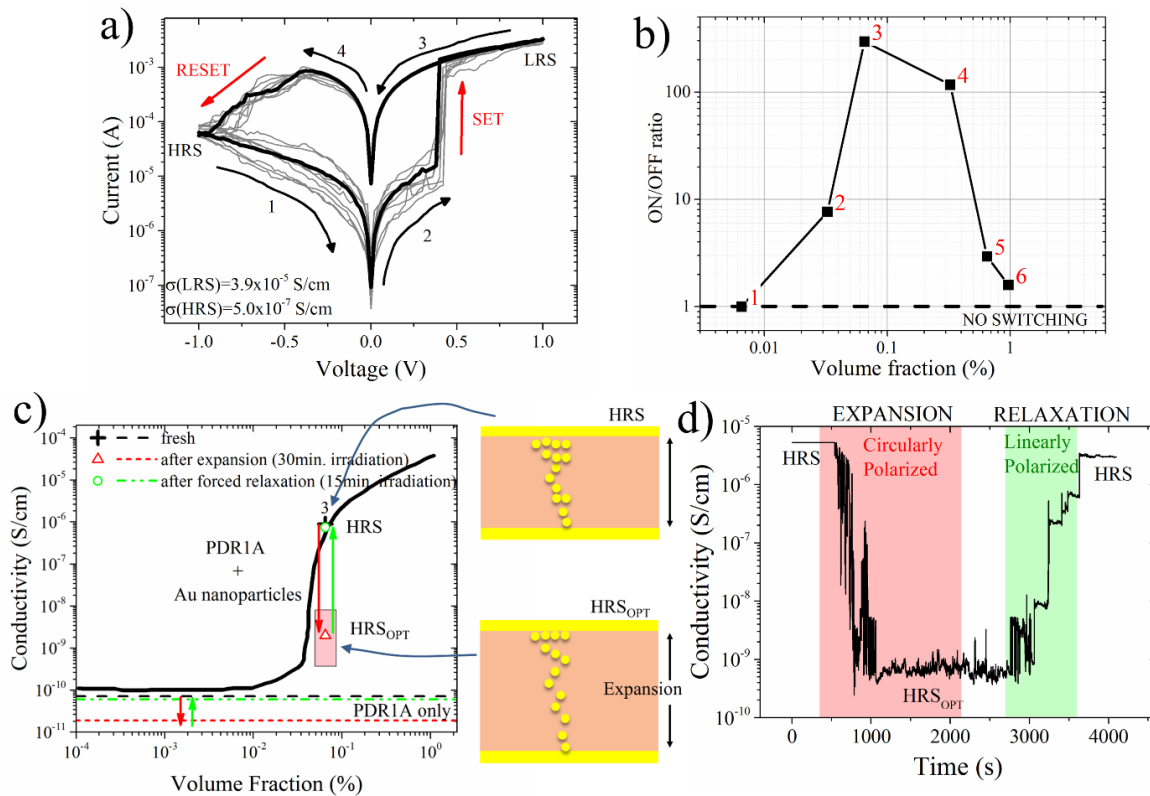
Figure 3. a) Repeated symmetric I-V characteristics of sample 3, between -1 V and +1 V; the sweep starts at -1V with the device found in its HRS; the corresponding conductivities for the HRS, σ_{HRS}, and LRS, σ_{LRS}, have been calculated by linear fitting the data. b) The ratio between the conductivities of the LRS and HRS states recorded on all samples considered in this work; a clear optimum (maximum) is identified for the sample just above the percolation threshold i.e. sample 3. c) The electrical conductivity (HRS) of sample 3 is shown before (black cross) and after (red triangle and arrow) expansion of the film as a result of irradiation by circularly polarized light. The red box indicates the range of observed HRS$_{opt}$ values due to statistical fluctuations. Irradiation with linear polarised light corrects the sample and restores the original conductivity (green circle and arrow). The black curve is a guide to the eye representing the conductivity versus nanoparticle volume fraction from Figure 2. The two schematics on the right illustrate that expansion of the film separates the particles across the film. The conductivity of the undoped PDR1A film is shown by dashed lines following similar optical cycling. d)

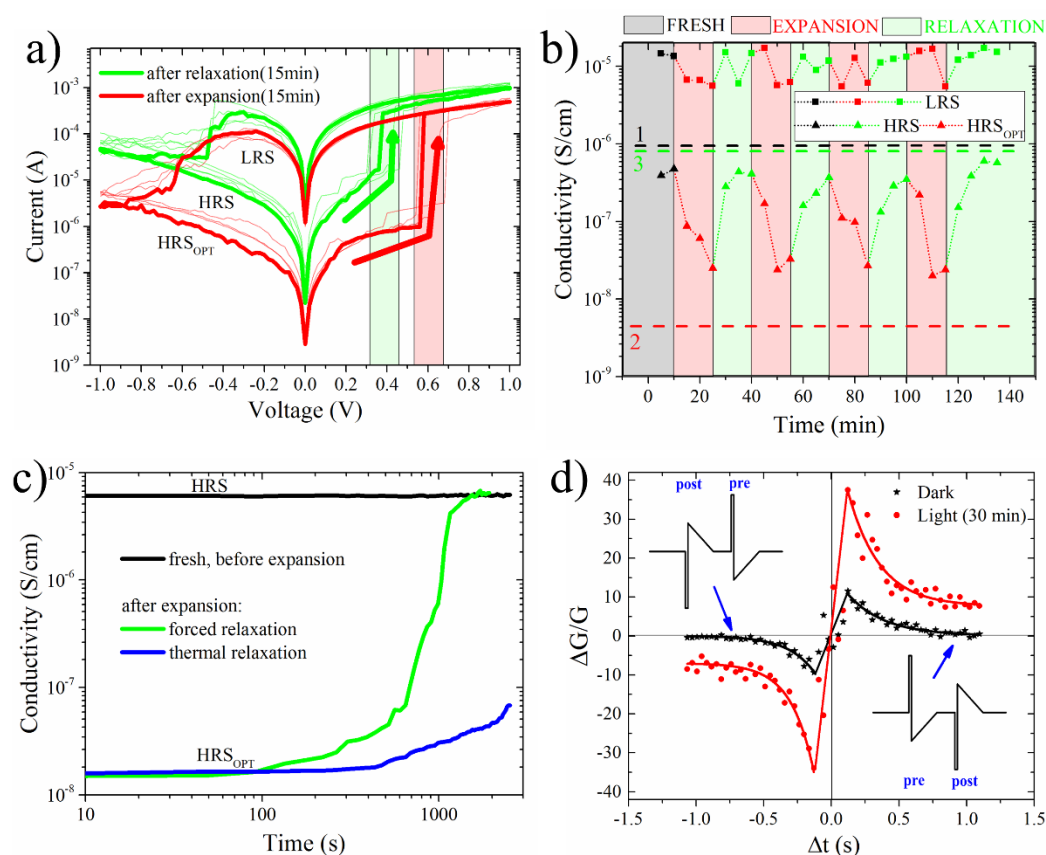Conductivity as a function of time during expansion and subsequent forced relaxation of the doped film.

Figure 4. a) A set of I-V characteristics of sample 3 recorded immediately after irradiation with circularly polarized light for 15 minutes (red lines) and again after subsequent irradiation with linearly polarized light for 15 minutes (green lines). b) The LRS, HRS and HRS$_{opt}$ conductivities are measured as a function of time during repeated irradiation of circularly and linearly polarized light of constant irradiance to expand and contract the film respectively. The dashed lines indicate the conductivity of the device in 1) its fresh, 2) fully expanded and 3) fully relaxed states. c) The time dependence of relaxation of HRS$_{opt}$ to HRS using linearly polarised irradiation (forced) and in the dark (thermal). Note there is some device variation in the actual conductivities, explaining discrepancies between conductivities measured in b) and c). d) Synaptic efficacy curves ($\Delta G/G$) for different separations of the pre- and post-synaptic pulse arrival time (Δt) are plotted for a fresh device and following irradiation by circularly polarized

light. The difference in the magnitude of the plots show that synaptic plasticity can be optically

modulated. The lines are fits to the asymmetric Hebbian STDP learning rule.[52]

The table of contents entry should be 50−60 words long, and the first phrase should be bold. The entry should be written in the present tense and impersonal style.

Keyword: Optical Switching Resistive Memory

Ayoub H. Jaafar,[a,b] Mary O'Neill,[a,c] Stephen M. Kelly,[d] Emanuele Verrelli[a,]* and Neil T. Kemp[a,]*

Percolation Threshold Enables Optical Resistive-Memory Switching and Light-Tuneable Synaptic Learning in Segregated Nanocomposites

ToC figure ((Please choose one size: 55 mm broad × 50 mm high **or** 110 mm broad × 20 mm high. Please do not use any other dimensions))
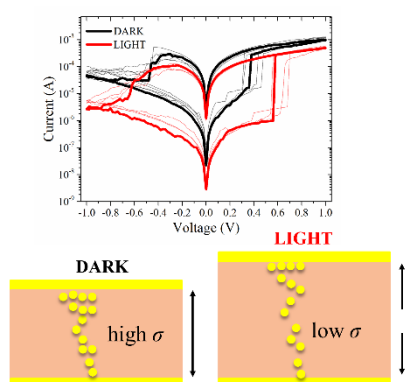
The resistance ratio between the low and high memory states of an optical memristor is photomechanically tuneable; photoexpansion breaks conducting nano-channels of gold nanoparticles doped in an azobenzene polymer so that the conductivity (σ) shifts from above to below a percolation threshold. The lifetime of the resistive memory states is also optically controllable, to enable spatial modulation of long and short term memory in an artificial synapse.

Supporting Information

Percolation Threshold Enables Optical Resistive-Memory Switching and Light-Tuneable Synaptic Learning in Segregated Nanocomposites

Ayoub H. Jaafar,[a,b] Mary O'Neill,[a,c] Stephen M. Kelly,[d] Emanuele Verrelli[a,*] and Neil T. Kemp[a,*]

[a] Department of Physics and Mathematics, University of Hull, Cottingham Rd, HU6 7RX, Hull, United Kingdom

[b] Physics Department, College of Science, University of Baghdad, Baghdad, Iraq

[c] School of Science and Technology, Nottingham Trent University, Clifton Lane, NG11 8NS, Nottingham, United Kingdom

[d] Department of Chemistry and Biochemistry, University of Hull, Cottingham Rd, HU6 7RX, Hull, United Kingdom

* Authors to whom correspondence should be addressed. Electronic mail:

N.Kemp@hull.ac.uk, E.Verrelli@hull.ac.uk

The solutions containing PDR1A and Au NPs used to fabricate the samples discussed in this work were obtained by blending two solutions, one containing dedecanethiol capped Au NPs and one PDR1A, with concentration of 1 % and 5 % by weight respectively. The solvent used for PDR1A was tetrahydrofuran and the solvent used for Au NPs was toluene. The blending ratio used to prepare the blend for each one of the samples discussed in this work was tuned in such a way that the final film would contain a predefined ratio by mass (R_M) of the two materials Au and PDR1A. The ratio by volume (R_V) and the volume fraction of the Au nanoparticles in PDR1A were then calculated using the following relations:

$$R_M = \frac{m_x}{m_y}\frac{C_x}{C_y}$$

Equation S1

$$R_V = \frac{\rho_{PDR1A}}{\rho_{Au}} R_M$$

Equation S2

$$Au\,Vol.frac. = \frac{1}{1 + \dfrac{1}{R_V}}$$

Equation S3

where x denotes the stock solution containing the Au nanoparticles, y the solution containing the PDR1A, C_x is 0.01 (1% wt) and C_y is 0.05 (5% wt), m_x and m_y represent the masses of the amount of stock solutions used to create a blend, R_M (R_V) provides the ratio by mass (volume) between the solutes Au and PDR1A in the blend. Regarding the density values in the above calculations, 19.3 g/cm^3 and 1.26 g/cm^3 were used for Au and PDR1A respectively. The samples prepared in this work are those listed in Table S1.

Table S1. Samples prepared in this work

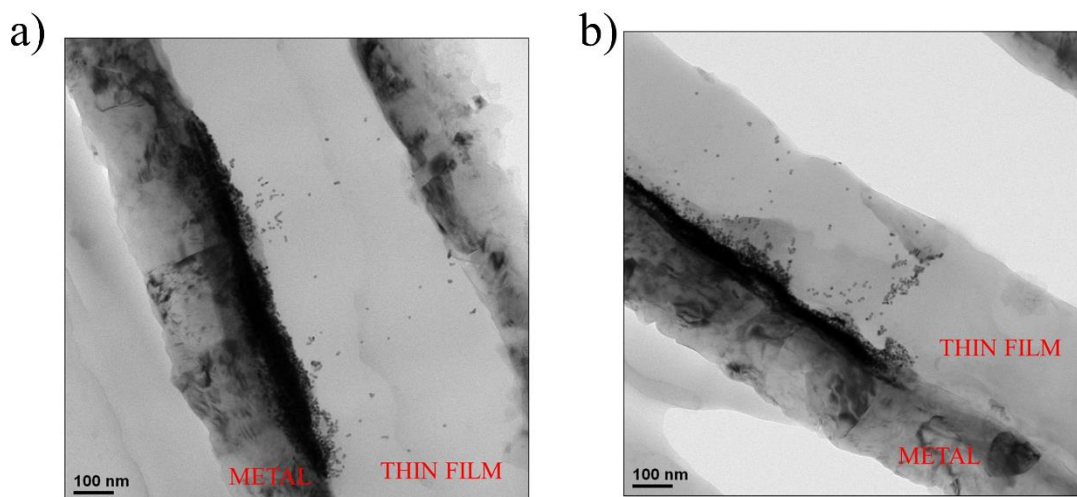| Sample	Ratio by mass R_M (Au:PDR1A)	Au Volume fraction (%) in PDR1A
PDR1A Reference	0	0
1	0.001	0.0065
2	0.005	0.033
3	0.01	0.065
4	0.05	0.33
5	0.1	0.65
6	0.15	0.97

a)

b)

Figure S1. TEM images of different areas of the same thin film of Au nanoparticle (NP) doped PDR1A which was annealed at 95 °C for 8 hours. The metal layer present in the left of the images is added after thermal annealing to protect the device structure during cross-sectioning by microtome. Both images show clustering of the NPs at what was the polymer/air interface. Most of the bulk of the film contains very few NPs but (b) shows a discrete region where the NPs extend across the bulk of the film. TEM after thermal annealing. In (b), the NPs are mostly located at the top Al interface.
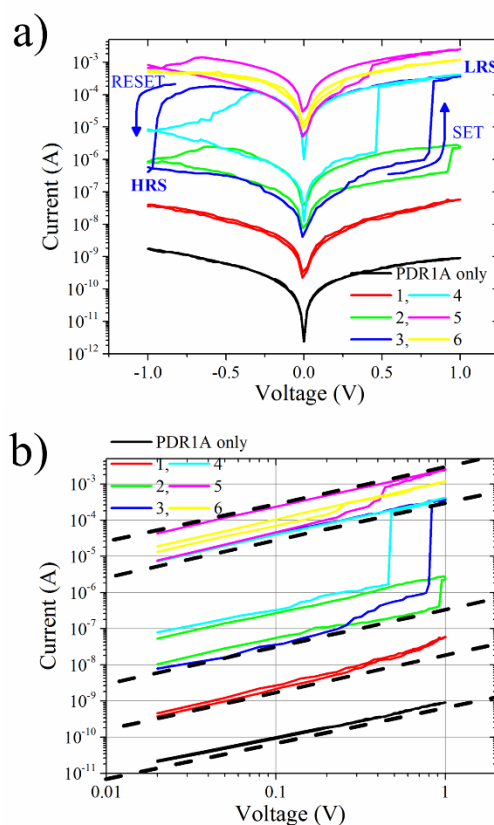
a)

b)

Figure S2. (a) log-linear and (b) log-log plots of the I-V characteristics from the PDR1A host and a set of Au NP doped samples with different NP concentrations. The NP concentration of samples 1 -6 is given in Table S1. The voltage is cycled as illustrated from the HRS state. The dashed black curve in (b) is a guide to the eye to indicate a purely ohmic behaviour.
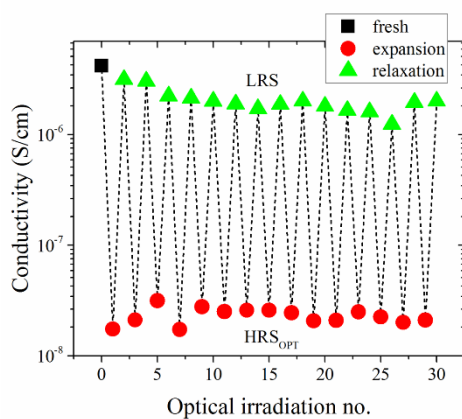

Figure S3. Optical cycling showing consistent and reproducible switching of the conductivity of the optical memristor device.